

Scaling of the spin Seebeck effect in bulk and thin film

By K. Morrison,^{1*} A.J Caruana,^{1,2} C. Cox¹ & T.A. Rose¹

[*] Dr K. Morrison

¹Department of Physics, Loughborough University,
Loughborough LE11 3TU (United Kingdom)

²ISIS Neutron and Muon Source, Didcot, Oxfordshire, OX11 0QX
E-mail: k.morrison@lboro.ac.uk

Keywords: Magnetic materials, thermoelectrics, thin films

PACS: 72.25.Mk, 72.25.-b, 75.76.+j

Whilst there have been several reports of the spin Seebeck effect to date, comparison of the absolute voltage(s) measured, in particular for thin films, is limited. In this letter we demonstrate normalization of the spin Seebeck effect for Fe₃O₄:Pt thin film and YIG:Pt bulk samples with respect to the heat flux J_q , and temperature difference ΔT . We demonstrate that the standard normalization procedures for these measurements do not account for an unexpected scaling of the measured voltage with area that is observed in both bulk and thin film. Finally, we present an alternative spin Seebeck coefficient for substrate and sample geometry independent characterization of the spin Seebeck effect.

I. INTRODUCTION

The spin Seebeck effect (SSE) is defined as the production of a spin polarized current in a magnetic material subject to a thermal gradient. It was first highlighted by Uchida *et al.* [1], and led to the development of a new field of magnetothermal effects (such as spin Peltier and spin Nernst) now grouped together under spin caloritronics [2].

Observation of the spin Seebeck effect is achieved by placing a heavy metal such as Pt in contact with the magnetic material, where the spin current generated in the magnetic layer is injected into the Pt layer and converted to a useable voltage by the inverse spin Hall effect [3,4]. The advantage of the SSE is that it can be used as a source of pure spin polarized current for spintronics applications, paving the way for a host of new devices (such as spin Seebeck based diodes) [5–8]. In addition to its potential applications in spintronics, it has been presented as an alternative to conventional thermoelectrics for harvesting of waste heat, due to decoupling of the electric and thermal conductivities that typically dominate the efficiency [9] [10] [11]. This is in part due to a completely different device architecture, such as that shown in Fig. 1, where the magnetic layer can be chosen to have low thermal conductivity independent of the second paramagnetic layer, which in turn can be selected to have low resistivity.

There are two measurement geometries for the spin Seebeck effect - longitudinal and transverse. In early work there was some comparison between the two with regards to substrate (phonon) contributions to the effect in thin films, and the impact of the anomalous Nernst effect [12]. In this work, however, we discuss the longitudinal SSE (LSSE) only (Figure 1(a)), since

this geometry lends itself readily to energy harvesting. Furthermore, the LSSE is largely absent of artefacts that arise from thermal shunting of the temperature gradient, i.e. where there is a mismatch between the thermal conductivity of the substrate and magnetic thin film [13].

Whilst there have been extensive studies of the spin Seebeck effect over the last 5-10 years, this has predominantly been in the YIG:Pt system, where for thin films, the substrate is often GGG [14] [15]. Reports of the spin Seebeck coefficient for this material system can, however, vary significantly [9]. Whilst this is sometimes attributed to the quality of the interface [14] there are indications that it could also be affected by an artefact of the measurement of ΔT [16], [17], [18].

Despite indications of the importance of heat flux in measurements [16], [17] [19], typically, longitudinal spin Seebeck measurements are characterized by measuring the voltage generated across two contacts (of a spin convertor layer), as the temperature difference across the substrate, magnetic layer, and Pt is monitored.

If such spin Seebeck devices are to be considered for power conversion - in particular as thin film devices - there needs to be a shift in metrology so that meaningful comparison of the material parameters can be made. This is of particular importance if we consider the impact that the quality of the magnet:Pt interface can have on the observed voltage (i.e. efficiency of spin injection) [14]. An intermediate step is to use a simple thermal model to estimate the temperature difference across the active (magnetic) layer, however, this is limited by the unknown thermal conductivity of the thin films (likely to differ from the bulk), and thermal interface resistances.

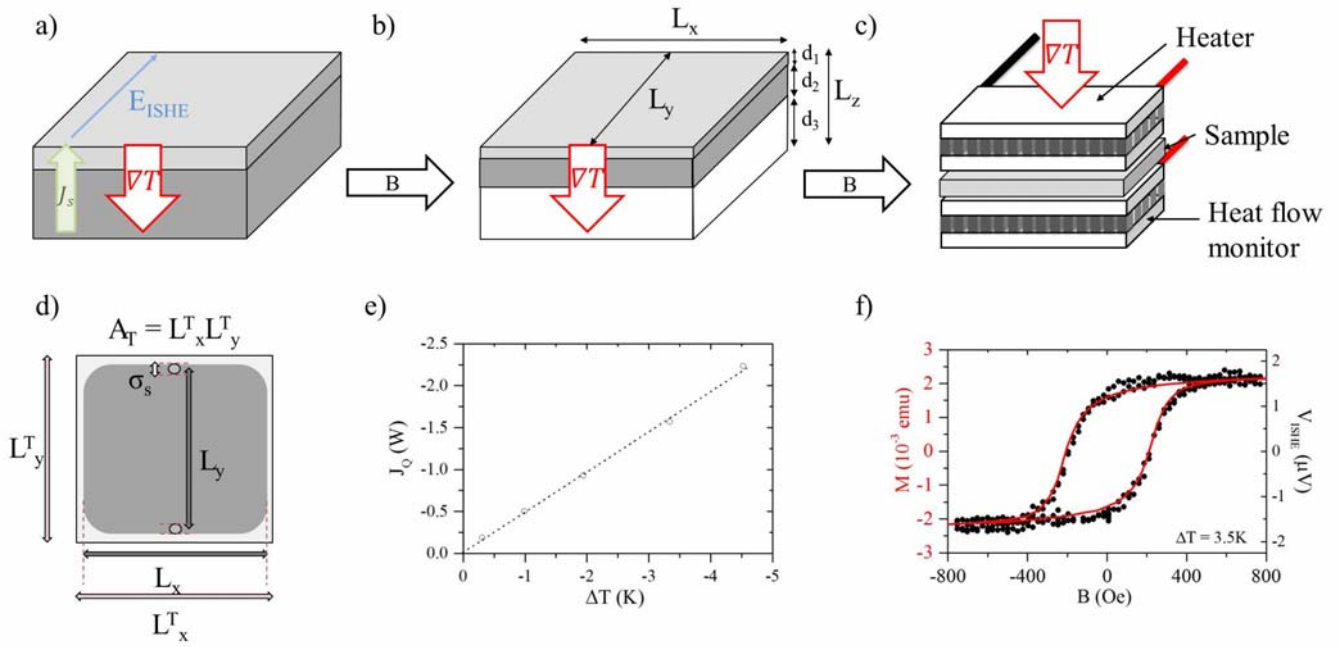


Figure 1. (a) Longitudinal spin Seebeck measurement geometries. Thermally generated spin current J_s , is produced in the magnetic layer (dark grey) and converted to a measurable voltage (E_{ISHE}) in the spin convertor layer (light grey) by the inverse spin Hall effect. (b) Typical longitudinal spin Seebeck thin film device; the length scales L_x , L_y , and L_z denote device dimensions with respect to the thermal gradient (along z axis). Individual thicknesses of each layer $\{d_1, d_2, d_3\}$ are also indicated. (c) Schematic of the experimental set-up used in this work. (d) Top view of a typical thin film device where active material may not cover the entire substrate. In this case, the thermal contact area is quantified by lengthscales L_x^T and L_y^T , active material width by L_x , and contact separation by $L_y \pm \sigma_s$, where σ_s denotes contact size. (e) Example of the linear relationship between heat flux, J_0 , and temperature difference, ΔT , in the measurements. (f) Example spin Seebeck data, V_{ISHE} (symbols) from 80 nm $\text{Fe}_3\text{O}_4:\text{Pt}$ thin film plotted alongside corresponding SQUID magnetometry (line).

In this paper we demonstrate the surprising result that the measured spin Seebeck voltage, V_{ISHE} , is proportional not only to the contact separation, L_y , and temperature difference, ΔT , but also the sample area, A_T . This manifests as an increase in V_{ISHE} in both thin film and bulk samples, suggesting that the spin Seebeck coefficient used to define the magnitude of the effect in a bilayer system needs to be redefined. We present examples of this scaling in both thin film and bulk samples and put forward a new coefficient suitable for normalizing the measured voltage for generic sample geometries.

II. EXPERIMENTAL METHOD

The thin film samples tested here were part of a series of 80:5 nm thick $\text{Fe}_3\text{O}_4:\text{Pt}$ bilayers deposited using pulsed laser deposition (PLD) in ultra-high vacuum (base pressure 5×10^{-9} mbar) onto 0.15 mm, 0.3 mm and 0.5 mm thick borosilicate glass and 0.6 mm or 0.9 mm fused silica substrates. The laser fluence and substrate temperature for Fe_3O_4 and Pt deposition were $1.9 \pm 0.1 \text{ J cm}^{-2}$ and $3.7 \pm 0.2 \text{ J cm}^{-2}$, and 400 C and 25 C, respectively. Fe_3O_4 was chosen due to its large spin polarization ($\sim 80\%$ [20]), low thermal conductivity (at 300 K: $\kappa_{thin\ film} \sim 2\text{-}3.5 \text{ W m}^{-1} \text{ K}^{-1}$, [21] $\kappa_{bulk} \sim 2\text{-}7 \text{ W m}^{-1} \text{ K}^{-1}$ [22]), and relative abundance of the constituent elements. Of particular note are the following: X-ray reflectivity data indicated a typical Pt thickness across the series of $4.5 \pm 0.5 \text{ nm}$ and a roughness $\sigma = 1.5 \pm 0.2 \text{ nm}$. Fe_3O_4 thickness was varied from 20 to 320 nm.

Further details are given in [19] and the supplementary information.

Bulk YIG was prepared by the solid state method [23]. Stoichiometric amounts of Y_2O_3 and Fe_2O_3 starting powders (Sigma Aldrich 99.999% and 99.995% trace metals basis, respectively) were ground and mixed together before calcining in air at 1050 °C for 24 hours. Approximately 0.5g of the calcined powder was then dry pressed into a 13 mm diameter, $1.8 \pm 0.2 \text{ mm}$ thick cylindrical pellet. The pellet was then sintered at 1400 °C for 12 hours, after which, it was checked by XRD prior to sputtering 5 nm of Pt onto the as prepared surface using a benchtop Quorum turbo-pumped sputter coater. Samples were cut to size thereafter, using an IsoMet low speed precision cutter. Average grain size for this polycrystalline sample (determined using scanning electron microscopy) was $14.5 \mu\text{m}$, with an open porosity of 30% measured by the Archimedes method. Further details are given in the supplementary information.

Magnetic characterization was obtained using a Quantum Design Magnetic Property Measurement System (SQUID) as a function of temperature and field. Room temperature coercive loops were confirmed for each sample using a Magneto-Optic Kerr effect (MOKE) magnetometer. Magnetometry of the Fe_3O_4 films at room temperature typically exhibited a coercive field $H_c = 197 \pm 5 \text{ Oe}$, saturation magnetization $M_s = 90 \text{ emu g}^{-1}$, and a remanent moment of $M_r = 68 \text{ emu g}^{-1}$. Magnetometry of the YIG pellet exhibited a a coercive field $H_c = 7 \text{ Oe}$, saturation magnetization $M_s = 25 \text{ emu g}^{-1}$, and a remanent moment of $M_r = 3 \text{ emu g}^{-1}$.

Spin Seebeck measurements were obtained from a set-up similar to that of Sola *et al.* [16] and optimized for 12x12 and 40x40 mm samples. The thin film was sandwiched between 2 Peltier cells, where the top Peltier cell (1) acted as a heat source, and the bottom Peltier cell (2) monitored the heat Q , passing through the sample. The Peltier cells were calibrated by monitoring the Peltier voltage V_P , generated as a current was passed through surface mount resistors fixed to the top side of the Peltier cell (where the sensitivity S_p of the 12x12 and 40x40 mm set-ups was 0.12 V W^{-1} and 0.11 V W^{-1} , respectively at 300K). Two type E thermocouples mounted on the surface of the Peltier cells (such that they are in contact with the sample during the measurement) monitored the temperature difference across the sample, ΔT ; a schematic of this set-up is given in Fig. 1(c). Further information on calibration is given in the supplementary information.

III. THEORY

It is useful at this point to note some key characteristics of the SSE measurement. First, the voltage has been shown (for a single device) to increase linearly with temperature difference (ΔT) [10] or heat flux (J_Q) [16]. Secondly, it is known to increase linearly with contact separation (L_y) [10]. Lastly, for thin films, there have been indications of a length scale of the order of the magnon free path length above which the voltage generated saturates [24] [25].

In response to these observations, some of the first attempts to quantify the SSE were to normalize the voltage measured, V_{ISHE} , to the temperature difference ΔT ,

$$S_1 = \frac{V_{ISHE}}{\Delta T} \quad (1)$$

where the units are ($\mu\text{V K}^{-1}$). More accurately, this could also be normalized to contact separation L_y ,

$$S_2 = \frac{V_{ISHE}}{L_y \Delta T} \quad (2)$$

with units of ($\mu\text{V K}^{-1} \text{m}^{-1}$).

Given that the spin Seebeck effect is often defined in terms of the thermal gradient across the magnetic material ∇T , the spin Seebeck coefficient is more often defined as,

$$S_3 = -\frac{E_{ISHE}}{\Delta T} = \frac{V_{ISHE} L_z}{L_y \Delta T} \quad (3)$$

where the units are ($\mu\text{V K}^{-1}$), and the thermal gradient ∇T can be described by the temperature difference ΔT , divided by the thickness of the sample L_z .

It was shown recently by Sola *et al.*, that there is the added complication of thermal resistance between the sample and the hot and cold baths (i.e. the interface across which ΔT is measured) [17]. Here they showed in measurements of the same sample in an experimental set-up at both INRIM and Bielefeld that the measurement as a function of ΔT was unreliable – differing by a factor of 4.6 (gave $S_3 = 0.231 \mu\text{V K}^{-1}$ and $0.0496 \mu\text{V K}^{-1}$, respectively), whereas by normalizing to heat flux, both set-ups obtained the same value to within 4% ($S_3 = 0.685$ and $0.662 \mu\text{V K}^{-1}$, respectively).

In this work they measured the heat flux, J_Q , using a calibrated Peltier cell and initially determined the normalized voltage generated per unit of heat flux,

$$S_4 = \frac{V_{ISHE}}{L_y \left(\frac{Q}{A_T} \right)} \quad (4)$$

where Q is the heat passing through a sample with cross-sectional area surface A_T , and the units are ($\mu\text{V m W}^{-1}$). Given that the thermal conductivity can be defined by,

$$\kappa = \left(\frac{Q}{A_T} \right) / \left(\frac{\Delta T}{L_z} \right) \quad (5)$$

where $J_Q = Q/A_T$, they argued that S_3 (equation 3) could be estimated by multiplying S_4 (equation 4) by κ . This was based on using a simple linear model that assumed that the thermal conductivity of the substrate and magnetic film were well matched.

For samples where this is not the case (the thermal conductivity is not well matched), we showed that the substrate can play a significant role in determining the value of ΔT across the active material – the magnetic layer – in a thin film device [19]. This highlights a significant disadvantage of using the spin Seebeck coefficients outlined in equations (1)-(3) for thin film devices. To circumvent this problem, we argued that in the equilibrium condition a simple thermal model can be used to determine the heat flux through the entire sample,

$$Q = \frac{A_T \Delta T}{\left(\frac{d_1}{\kappa_1} \right) + \left(\frac{d_2}{\kappa_2} \right) + \left(\frac{d_3}{\kappa_3} \right)} \quad (6)$$

where $\{d_1, d_2, d_3\}$ and $\{\kappa_1, \kappa_2, \kappa_3\}$ are the thicknesses and thermal conductivities of the top layer (1), FM layer (2) and substrate (3), respectively; and ΔT is the temperature difference across the entire device. It can be seen from

this, that the temperature gradient is a function of the thermal conductivities of each layer and that the temperature difference across the ‘active’ magnetic layer can be thermally shunted by substrates with relatively low thermal conductivities (for example, see the comparison made between SrTiO₃ and glass Fe₃O₄:Pt in [19]). Note that this treatment of the thermal profile is, an oversimplification as it does not take into account any temperature drops at interfaces.

Given that J_Q will be constant across the sample once thermal equilibrium has been reached, and that it will be proportional to the temperature gradient across the active magnetic layer, of thickness d_2 , we can write the thermal gradient as,

$$\nabla T = \frac{\Delta T}{d_2} = \frac{J_Q}{d_2} \left(\frac{d_2}{\kappa_2} \right) = \frac{J_Q}{\kappa_2} \quad (7)$$

where for the magnetic layer $L_z=d_2$ and we now have a direct relationship between the thermal gradient, ∇T , and the heat flux J_Q in the active material.

Finally, whilst there has been limited discussion of the scaling of the spin Seebeck effect, it was argued by Kirihaara *et al.*, that the spin Seebeck effect may also scale with area [26] based on the change in internal resistance of the paramagnetic layer,

$$R_0 = \frac{\rho L_y}{L_x t_{Pt}} \quad (8)$$

where ρ is the resistivity, t_{Pt} is the thickness, and L_x is the width of the Pt layer. This suggests that the maximum power extracted is,

$$P_{max} \propto \frac{V^2}{R_0} \propto L_x L_y \quad (9)$$

Note that this observation would only indicate an increase in power output of the bilayer (not the voltage).

IV. RESULTS AND DISCUSSION

To test normalization of the spin Seebeck measurements for both heat flux and sample area, we prepared several Fe₃O₄:Pt samples on glass substrates of varying thickness, where the Pt thickness was kept constant at 5 nm (± 0.5 nm) in order to minimize any variation in the observed voltage, V_{ISHE} , due to the inverse spin Hall effect [19]. V_{ISHE} was then measured for various thermal gradients as a function of applied magnetic field.

We first took one of the Fe₃O₄:Pt samples from our study (22x22x0.5 mm glass substrate, 80 nm Fe₃O₄, 5 nm Pt) and measured it in various orientations, as summarized in Figure 2(a)&(b).

To increase the area of the measured sample, a buffer layer between the two Peltier cells was introduced (substrate of same thickness as the sample – on the assumption that control of J_Q by the magnetic layer is largely negligible). This effectively increased the thermal contact area A_T , by increasing $\{L_x^T, L_y^T\}$ whilst $\{L_x, L_y, L_z\}$ were fixed (see Figure 1(d)). Secondly, the 22x22 mm sample was cleaved in two and measured along the long and short sides, thus changing A_T , the aspect ratio and L_y . Errors were determined from the combination of uncertainty in contact separation L_y , thermal contact area A_T , and the noise floor of the V_{ISHE} voltage.

Fig. 2(a) shows the calculated spin Seebeck coefficients S_2 (left) and S_4 (right axis) as the area, A_T , was increased. Initially this data suggests that there appears to be an increase in the coefficient measured by the heat flux method (S_4), but not by the temperature difference method (S_2). In other words, for the same sample, the aspect ratio and total area could have an impact on the determination of S_4 . In addition, by plotting S_4 against various combinations of L_x^T , L_y^T , and A_T (as shown in Figure 3), we found that the only way to reduce the measurement to a constant value was to divide through by $A_T^{0.5}$. This is further demonstrated by the linear dependence observed for the thin film data in Figure 2(b). Note that it also accounts for areas of non-active sample.

Given that in the steady state, $S_4 \kappa = S_2$ (equations 2-7), this mismatch between S_2 and S_4 indicates that there is a measurement artefact that needs to be resolved. To test for this, we also measured bulk samples as a function of A_T , where the temperature difference across the active material would now be an order of magnitude larger (than our thin films) and thus, less prone to errors such as interface (thermal) resistance.

Figure 2(c)&(d), shows the same normalization measurements for the bulk YIG:Pt sample as a function of A_T . Here, the sample was measured in both the 12x12 mm and 40x40 mm sample holders, and cut from the original 13 mm pellet to various sizes. Notice that the data from the 12x12 mm and 40x40 mm measurement set-ups are the same within error, and that it still indicates scaling with $A_T^{0.5}$. For this dataset, plotting S_4 as a function of L_x^T also indicated a linear trend (as seen in Figure (4)), but this is for the case where $A_T=L_x L_y$ (as $L_x^T=L_x$ and $L_y^T=L_y$), i.e. it does not account for non-standard geometries, where the contacts are not necessarily at the edges of the sample. In either case, there is still a pronounced increase in the measured voltage as the sample size increases, that is not accounted for by normalizing simply by contact separation, or resistance.

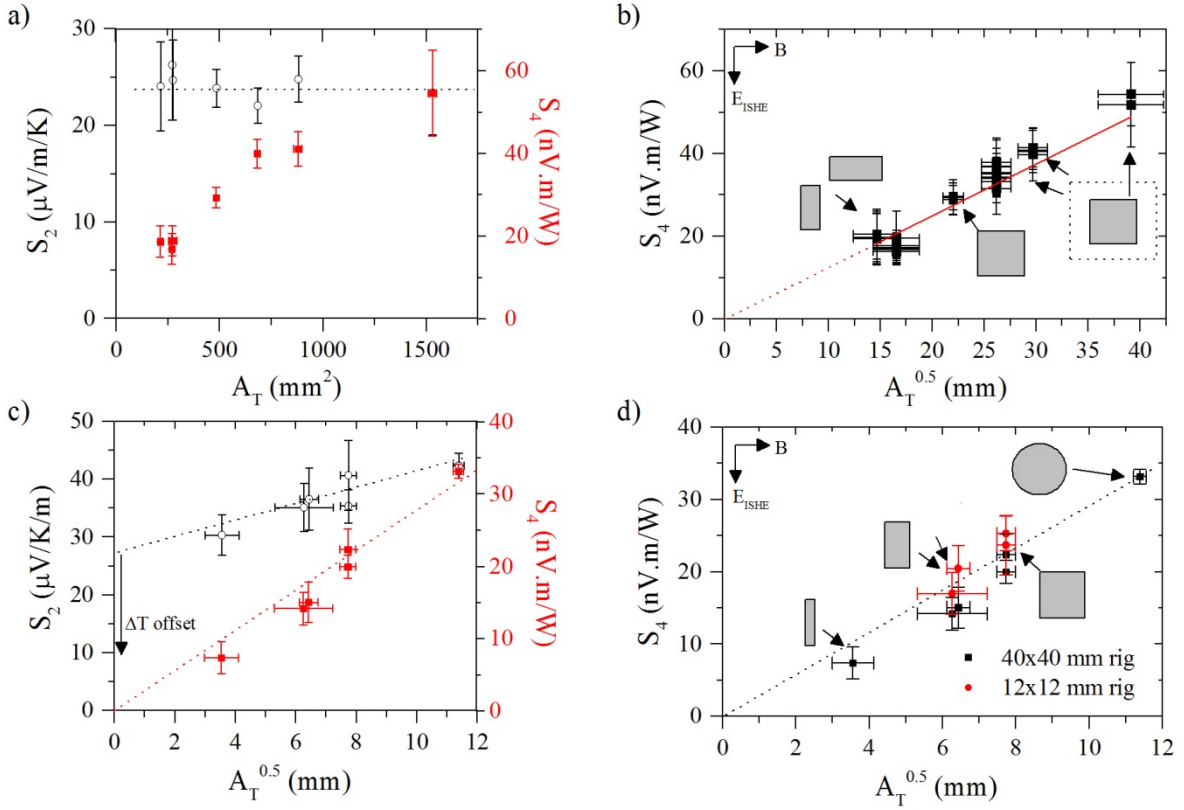


Figure 2 Summary of normalization measurements for thin film $\text{Fe}_3\text{O}_4\text{:Pt}$ (top) and bulk polycrystalline YIG:Pt (bottom). (a)&(c) S_2 (open symbols) and S_4 (closed symbols) as a function of A_T (as L_z is fixed S_2 and S_3 are equivalent). (b)&(d) S_4 as a function of $A_T^{0.5}$. Inset sketches indicate aspect ratio for the individual data points. For the thin film measurements a buffer layer (same thickness glass substrate) was inserted in order to increase A_T ; as indicated by the inset sketch with dotted outline.

For the bulk samples, however, there is now also indication of scaling of the temperature difference method (S_2) with $A_T^{0.5}$. We argue that the reason for this is that the temperature difference across the active material is now no longer masked by thermal interface offsets. This can be seen in Figure 2(c), where S_2 as a function of $A_T^{0.5}$ indicates linear behavior, and a finite y-intercept. To understand the origin of the intercept, if we rewrite equation (2) to include the systematic error in measurement of ΔT we should have,

$$S_2' = \frac{V_{\text{ISHE}}}{L_y(\Delta T + \Delta T_{\text{offset}})} \quad (10)$$

where for the true measurement of S_2 , the temperature offset, ΔT_{offset} , should be subtracted. Given that for the measurements performed here there is no significant change in the interface layer (thermal grease + clamping of the sample in the set-up), it is reasonable to assume that ΔT_{offset} will be approximately constant (for same Q). As A_T is increased, however, ΔT across the sample will decrease, as can be seen from equation (5). This would lead to a decrease in S_2' , unless it also scales with $A_T^{0.5}$, which, given the corresponding data for S_4 , appears to be the case here.

We argue that this behavior was not observable in the thin film sample as the temperature difference across the active material, ΔT_2 , is of the order of 0.01% of the total measured ΔT . [19] As a result, there is competition between the increase in S_2 as A_T increases, and decrease in S_2 due to ΔT_{offset} . As stated earlier, the advantage of defining a spin Seebeck coefficient dependent on J_Q rather than ΔT is that it will be independent of thermal contact resistance [16], and the substrate.

Overall, for the bulk YIG measurements, normalizing to $A_T^{0.5}$ we obtain $S_2/A_T^{0.5} = 1.73 \pm 0.24$ mV/K/m² and $S_4/A_T^{0.5} = 2.4 \pm 0.34$ $\mu\text{V/W}$. These values are reasonable given that the thermal conductivity of YIG is expected to be 7 W/m/K for single crystal and that the thickness of the pellet was 1.8 ± 0.2 mm. For comparison, measurements of bulk polycrystalline YIG by Saiga *et al.*, [27] found S_I of up to 5 $\mu\text{V/K}$, when annealing to improve the interface equality. Given the same dimensions $L_x = 5$ mm, $L_y = 2$ mm, $L_z = 1$ mm, this amounts to $S_2 = 1000$ $\mu\text{V/K/m}$ and $S_2/A_T^{0.5} = 316$ mV/K/m², or $S_4/A_T^{0.5} = 45$ $\mu\text{V/W}$ (assuming $\kappa = 7$ W/m/K). If we compared to direct heat flux measurements by Sola *et al.*, with thin film YIG on

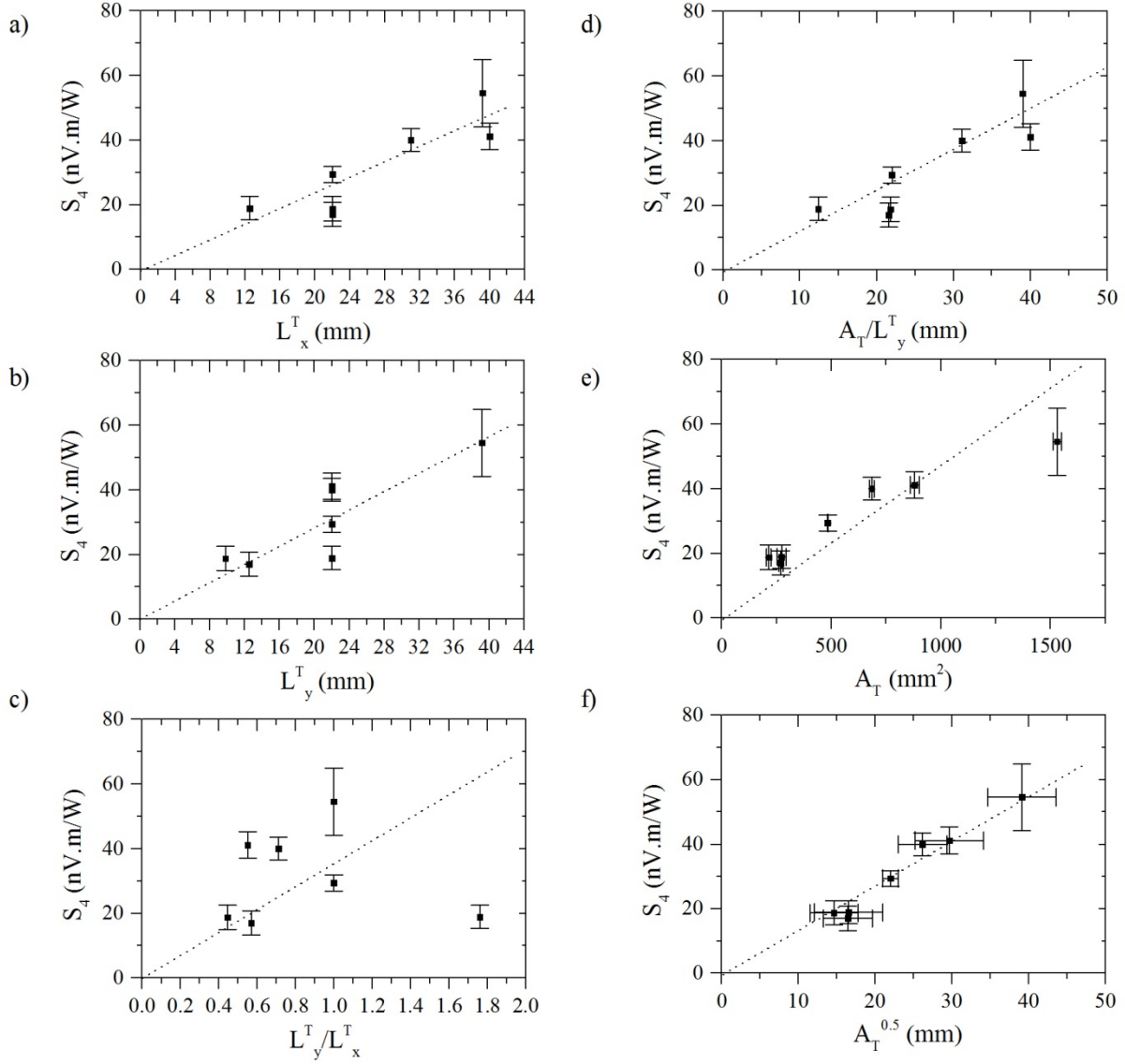


Figure 3 (a) – (f) Spin Seebeck measurement(s) for the $\text{Fe}_3\text{O}_4:\text{Pt}$ thin film as $A_T (=L_x^T L_y^T)$, L_x and L_y were varied, plotted against L_x^T , L_y^T , L_y^T/L_x^T , A_T/L_y^T , A_T and $A_T^{0.5}$.

GGG [17], they measured $0.11 \mu\text{V.m/W}$ for a 5×2 mm sample. Hence, $S_4/A_T^{0.5} = 34 \mu\text{V/W}$. Whilst these values are an order of magnitude larger than our measurement, for these examples care was taken to maximize the interface quality. In addition, the Pt thickness was smaller ($t_{\text{Pt}} < 3$ nm), which would be expected to also increase V_{ISHE} .

The implication of this $A_T^{0.5}$ scaling is that the voltage measured by typical spin Seebeck measurements is proportional to the heat available between the electrical contacts (L_y). Whilst an accumulation of spin current due to the spin Seebeck effect in the magnetic layer may be proportional to $\Delta T/L_z$, as detection relies on spin injection in the Pt layer for inverse spin Hall effect, the voltage will scale with $Q/A_T^{0.5}$ rather than Q/A . Therefore, to compare bilayer measurements of the spin Seebeck effect, the contact area, A_T must also be accounted for.

This is contrary to any scaling effect that you might expect due to changes in the resistance of the Pt layer (which might alter the power/voltage as L_x is constrained below a critical value). This is effectively demonstrated if you consider the upper right panel of Figure 2(b), where S_4 is plotted as the thermal contact area is increased, but the actual sample size is constant. In this case, S_4 continues to increase as $A_T^{0.5}$ is increased despite there being no additional magnetic material.

In addition, we also performed measurements on a sample with fixed area, A_T , but modifying L_x and L_y by scribing away areas of the sample (so that it can be considered as thermally connected but electrically isolated). In this case, V_{ISHE} always scaled with L_y , as typically expected for a measurement where A_T does not change.

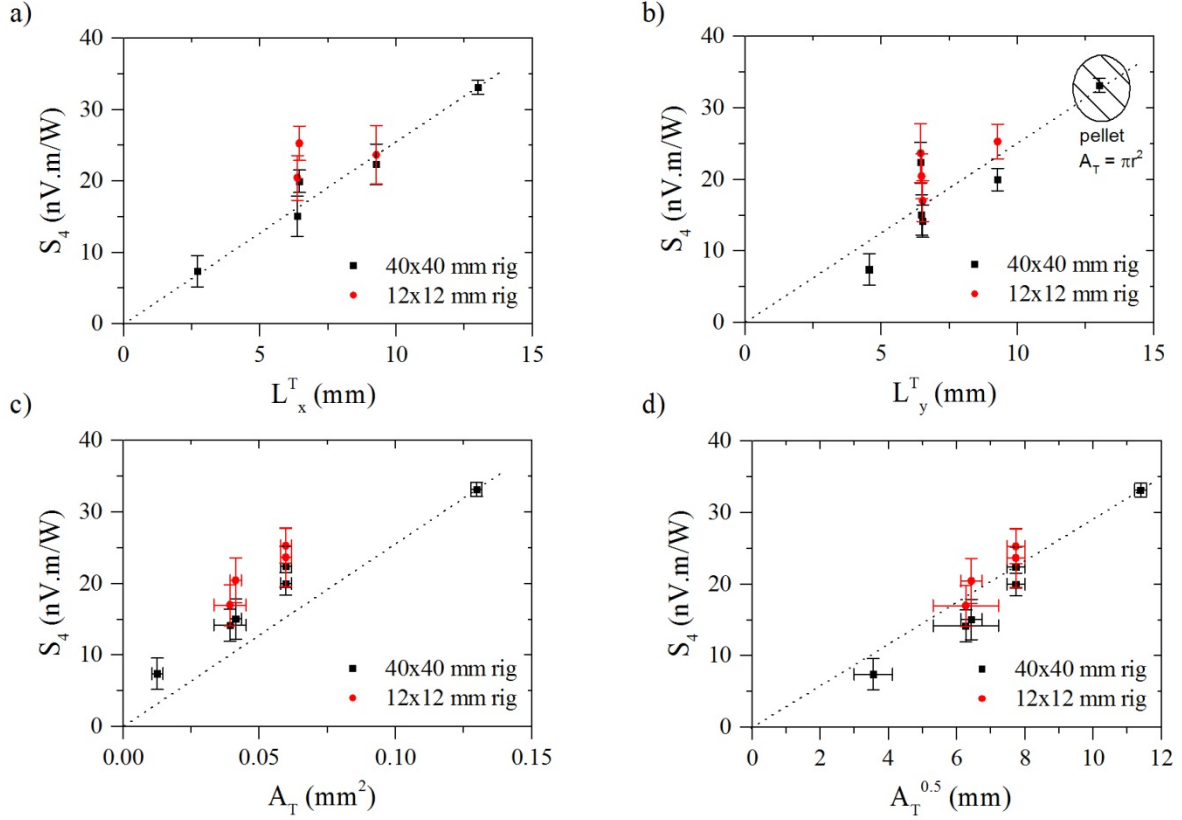


Figure 4 (a) – (d) Spin Seebeck measurement(s) of YIG:Pt as $A_T (=L_x^T L_y^T)$ except where sample was 13 mm pellet), L_x^T and L_y^T were varied, plotted against L_x^T , L_y^T , A_T and $A_T^{0.5}$.

Lastly, if you consider the impact of changing the sample area with respect to Q and ΔT (equation 6) you can see that for fixed ΔT (where we expect V_{ISHE} to be constant for same L_y), if A_T is increased, then Q is also increased. Whilst the heat flux, J_Q , might be constant, the heat available per unit length in L_y is not. Unless E_{ISHE} were to increase as A_T was increased, this can only be resolved by quantifying the spin Seebeck coefficient in terms of voltage generated per Watt (thus normalizing out contact separation and heat flux in a consistent way).

To further demonstrate the impact of thermal resistance on the measurement of S_2 , we show in Figure 5, results of spin Seebeck measurements for our Fe_3O_4 :Pt bilayers as a function of substrate and Fe_3O_4 thickness ($t_{\text{substrate}}$ and $t_{\text{Fe}_3\text{O}_4}$ respectively). Note that there was a scatter in our individual data points that can be attributed to varying thermal resistance between repeated measurements for the same sample; this led to larger error bars. In Figure 5(a) we show a summary of all measurements as a function of substrate thickness. As can be seen, S_2 decreased linearly with increasing thickness, as a larger proportion of ΔT was shunted across the substrate. As soon as the data was normalized for J_Q ($S_4/A_T^{0.5}$), as is also shown in Fig. 5(a) we obtained a relatively constant value (within error, and any

variation that might be expected is due to interface quality [14] or small differences in t_{Pt} and the resistance).

With regards to the thickness dependence of the spin Seebeck effect (Figure 5(b)) we also see collapse of the data onto the expected saturation at around 80 nm. This data shows that for these Fe_3O_4 :Pt bilayers $S=S_4/A_T^{0.5}=1.5\pm 0.1 \mu\text{V W}^{-1}$.

V. CONCLUSION

To summarize, we have demonstrated that the heat flux method is suitable for obtaining substrate independent measurements of the spin Seebeck effect, where the thermal conductivity of the thin film need not be known, and have proposed an alternative spin Seebeck coefficient for comparison of different material systems. By measuring the spin Seebeck effect as the thickness of the substrate, Fe_3O_4 layer and sample dimensions $\{L_x, L_y, A_T\}$ were varied, we demonstrated that for the same material system (assuming t_{Pt} is constant at 5 nm) that this method reliably returned a value of $1.5\pm 0.1 \mu\text{V W}^{-1}$. Since this result holds for different values of $t_{\text{substrate}}$, the heat flux normalization method could, therefore, be used to compare similar samples where the substrate thickness or type were varied. This would thus be a useful metric for comparison of prospective material systems (for application).

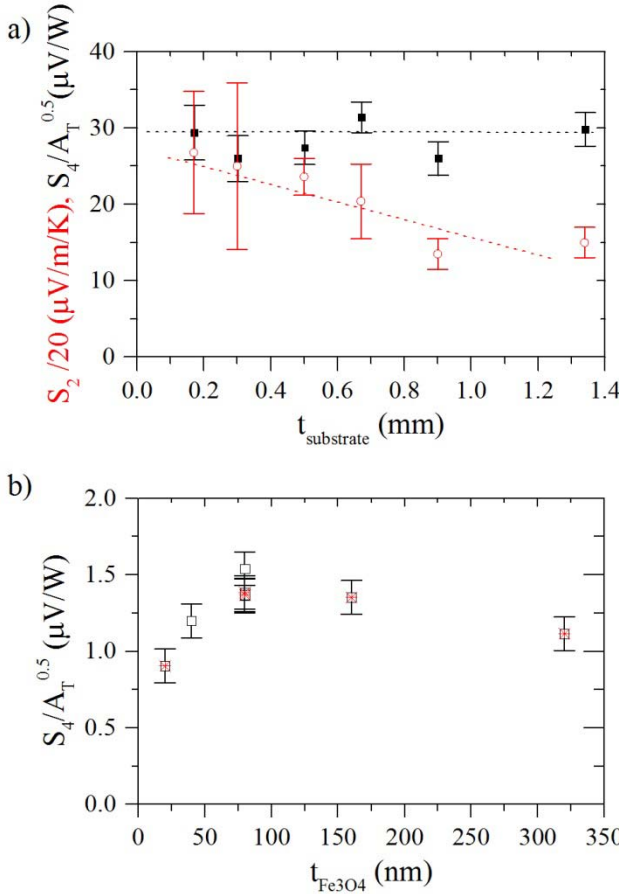


Figure 5 Summary of measurements as a function of substrate and Fe_3O_4 thickness, $t_{\text{substrate}}$ and $t_{\text{Fe}_3\text{O}_4}$, respectively. (a) Average value for S_2 (open symbols) and $S_4/A_T^{0.5}$ (closed symbols) as a function of the substrate thickness, $t_{\text{substrate}}$. (d) $S_4/A_T^{0.5}$ as a function of $t_{\text{Fe}_3\text{O}_4}$.

Lastly, we demonstrated a $A_T^{0.5}$ scaling of the spin Seebeck coefficient (as typically defined in the literature) and argue that this is a result of renormalizing to heat flow per unit area, when the measurement is constrained to a simple voltage per unit length. These results demonstrate that the voltage is proportional to the available energy per unit length (Q) - a result of spin injection into the paramagnetic layer before detection. It is likely that this relationship will break down as L_x is decreased toward the size of individual Fe_3O_4 grains, or increasing resistance, which could be the topic of future studies.

ACKNOWLEDGEMENTS

This work was supported by EPSRC First Grant (EP/L024918/1) and Fellowship (EP/P006221/1) and the Loughborough School of Science Strategic Major Operational Fund. KM would also like to thank M.D. Cropper for their help with use of the PLD system for sample fabrication and M Greenaway and J Betouras for useful discussions. Supporting data will be made available via the Loughborough data repository under doi 10.17028/rd.lboro.5117578.

APPENDIX A: HEAT LOSS CONSIDERATIONS

In an ideal case, the sample area would be chosen such that it matches the area of the hot and cold bath(s) in the measurement. Given that this paper studies the impact of sample size (where A_T is varied), it could be argued that for samples where A_T is less than the area of the top and bottom Peltier cells, there are significant thermal losses (radiation and convection). This was monitored during measurement by plotting the change in the measured J_Q as a function of ΔT (see Figure 1(e)).

We consider here the potential impact of radiative losses, as defined by:

$$Q = \varepsilon\sigma A(T_h^4 - T_c^4) \quad (11)$$

where ε is the emissivity of the radiating surface ($\varepsilon = 1$ for a perfect radiator), σ is the Stefan-Boltzman constant ($\sigma = 5.67 \times 10^{-8} \text{ W}/\text{m}^2/\text{K}^4$), A is the radiating surface area, and T_h and T_c are the temperatures of the hot and cold (ambient) surfaces respectively. For the sample environment used in these measurements there will be 3 sources of radiative heat loss:

- 1) Top surface of the Peltier cell where the sample is not connected (forming a conductive path).
- 2) Bottom surface of the Peltier cell where sample is not connected.
- 3) The sides of the sample.

Sources 1&2 can be considered simultaneously given that A will be the same, and it is reasonable to assume that the majority of the heat lost from the top surface will be measured by the bottom surface (i.e. overestimating J_Q). Thus for 1&2:

$$Q_{\text{rad}} = \varepsilon\sigma(A_P - A_T)(T_h^4 - T_c^4) \quad (12)$$

where A_p is the Peltier area.

For the worst case scenario for radiative losses 1&2 the smallest samples measured in the $40 \times 40 \text{ mm}^2$ Peltier setup had $A_T = 100 \text{ mm}^2$. In this case, $A_P - A_T = 1500 \text{ mm}^2$. Inserting this into equation (12), the radiative heat loss would be $Q = 0.045 \text{ W}$ for a measured heat flow of 2.5 W (1.8%).

The worst case scenario for radiative loss via the sides of the sample was for the thickest samples, with largest area. The thickness of the measured thin films were 0.17-1.34 mm, with a maximum radiative area (from the sides) of 171.2 mm^2 . For a typical temperature difference of 5 K this would amount to radiative loss of approximately 0.0045 W (0.2% of Q). For the YIG samples, with thickness = 1.8 mm, and temperature differences of up to 25 K the radiative loss would be 0.012 W (0.5% of Q). In this context, for these temperature differences, radiative loss is negligible with respect to the changes seen as a function of $A_T^{0.5}$.

As a general rule of thumb, radiative heat losses in this system can be quickly assessed by monitoring J_Q vs. ΔT . Given equations (5) and (11), for the ideal case the heat flux through the sample should be linear with respect to ΔT . As soon as the radiative heat losses become significant with respect to the heat flow through the sample, this linearity breaks down as a larger J_Q will be observed per unit ΔT .

Conversely, for much thicker samples, where radiative loss from the sides of the sample starts to

become significant, such as is the case with the bulk YIG samples, heat loss would result in a lower measured J_Q per unit ΔT as well as non-linearity of $J_Q(\Delta T)$. We only present data for values of ΔT where this linearity was preserved.

REFERENCES

- [1] K. Uchida, S. Takahashi, K. Harii, J. Ieda, W. Koshibae, K. Ando, S. Maekawa, and E. Saitoh, *Nature* **455**, 778 (2008).
- [2] G. E. W. Bauer, E. Saitoh, and B. J. van Wees, *Nat. Mater.* **11**, 391 (2012).
- [3] T. Jungwirth, J. Wunderlich, and K. Olejnik, *Nat. Mater.* **11**, 382 (2012).
- [4] A. Hoffmann, *IEEE Trans. Magn.* **49**, 5172 (2013).
- [5] H.-H. Fu, D.-D. Wu, L. Gu, M. Wu, and R. Wu, *Phys. Rev. B* **92**, 45418 (2015).
- [6] J. Ren, J. Fransson, and J. X. Zhu, *Phys. Rev. B - Condens. Matter Mater. Phys.* **89**, 1 (2014).
- [7] L. Gu, H. H. Fu, and R. Wu, *Phys. Rev. B - Condens. Matter Mater. Phys.* **94**, 1 (2016).
- [8] S. Borlenghi, W. Wang, H. Fangohr, L. Bergqvist, and A. Delin, *Phys. Rev. Lett.* **112**, 47203 (2014).
- [9] K. I. Uchida, H. Adachi, T. Kikkawa, A. Kirihara, M. Ishida, S. Yorozu, S. Maekawa, and E. Saitoh, *Proc. IEEE* **104**, 1946 (2016).
- [10] K. Uchida, M. Ishida, T. Kikkawa, a Kirihara, T. Murakami, and E. Saitoh, *J. Phys. Condens. Matter* **26**, 343202 (2014).
- [11] S. R. Boona, S. J. Watzman, and J. P. Heremans, *APL Mater.* **4**, (2016).
- [12] M. Schmid, S. Srichandan, D. Meier, T. Kuschel, J.-M. Schmalhorst, M. Vogel, G. Reiss, C. Strunk, and C. H. Back, *Phys. Rev. Lett.* **111**, 187201 (2013).
- [13] S. Y. Huang, W. G. Wang, S. F. Lee, J. Kwo, and C. L. Chien, *Phys. Rev. Lett.* **107**, 216604 (2011).
- [14] Z. Qiu, D. Hou, K. Uchida, and E. Saitoh, *J. Phys. D. Appl. Phys.* **48**, 164013 (2015).
- [15] T. Kikkawa, K. Shen, B. Flebus, R. A. Duine, K. I. Uchida, Z. Qiu, G. E. W. Bauer, and E. Saitoh, *Phys. Rev. Lett.* **117**, 207203 (2016).
- [16] A. Sola, M. Kuepferling, V. Basso, M. Pasquale, T. Kikkawa, K. Uchida, and E. Saitoh, *J. Appl. Phys.* **117**, 17C510 (2015).
- [17] A. Sola, P. Bougiatioti, M. Kuepferling, D. Meier, G. Reiss, M. Pasquale, T. Kuschel, and V. Basso, *Sci. Rep.* **7**, 1 (2017).
- [18] R. Iguchi, K. Uchida, S. Daimon, and E. Saitoh, *Phys. Rev. B* **95**, 174401 (2017).
- [19] A. J. Caruana, M. D. Cropper, J. Zipfel, Z. Zhou, G. D. West, and K. Morrison, *Phys. Status Solidi - Rapid Res. Lett.* **10**, 613 (2016).
- [20] Y. S. Dedkov, U. Rüdiger, and G. Güntherodt, *Phys. Rev. B* **65**, 64417 (2002).
- [21] N.-W. Park, W.-Y. Lee, J.-A. Kim, K. Song, H. Lim, W.-D. Kim, S.-G. Yoon, and S.-K. Lee, *Nanoscale Res. Lett.* **9**, 96(8pp) (2014).
- [22] G. A. Slack, *Phys. Rev.* **126**, 427 (1962).
- [23] P. Grosseau, a. Bachiarrini, and B. Guilhot, *Powder Technol.* **93**, 247 (1997).
- [24] A. Kehlberger, U. Ritzmann, D. Hinzke, E.-J. Guo, J. Cramer, G. Jakob, M. C. Onbasli, D. H. Kim, C. A. Ross, M. B. Jungfleisch, B. Hillebrands, U. Nowak, and M. Kläui, *Phys. Rev. Lett.* **115**, 96602 (2015).
- [25] A. Anadon, R. Ramos, I. Lucas, P. A. Algarabel, L. Morellon, M. R. Ibarra, and M. H. Aguirre, *Appl. Phys. Lett.* **109**, 12404 (2016).
- [26] A. Kirihara, K. Uchida, Y. Kajiwara, M. Ishida, Y. Nakamura, T. Manako, E. Saitoh, and S. Yorozu, *Nat. Mater.* **11**, 686 (2012).
- [27] Y. Saiga, K. Mizunuma, Y. Kono, J. C. Ryu, H. Ono, M. Kohda, and E. Okuno, *Appl. Phys. Express* **7**, 93001 (2014).

Supplementary information for “Scaling of the spin Seebeck effect in bulk and thin film”

K. Morrison¹, A J Caruana^{1,2}, C. Cox¹, T.A Rose¹

¹ Department of Physics, Loughborough University, Loughborough, LE11 3TU, United Kingdom

² ISIS Neutron and Muon Source, Didcot, Oxfordshire, OX11 0QX

Keywords Magnetic materials, thermoelectrics, thin films

1 Introduction Extensive experimental details and additional characterization of the films presented in “Scaling of the spin Seebeck effect in bulk and thin film” is given in this supplementary information.

Additional X-ray diffraction (XRD), resistivity and X-ray reflectivity (XRR) data is used to demonstrate the quality of Fe₃O₄ thin films – exhibiting the characteristic Verwey transition for this phase[1], as well as the expected magnetic characteristics as a function of temperature. This is followed by additional XRD, and XRR data for the Fe₃O₄:Pt bilayers to further demonstrate the magnetic and structural quality of the films, as well as XRD and SEM data of the YIG pellet chosen for this study. Finally, further details of the spin Seebeck measurements are given, alongside the additional ‘scribing’ study data.

2 Experimental Details

2.1 Sample preparation

The series of films prepared for this study are listed in Table S1. They were prepared in vacuum (base pressure of 5×10^{-9} mbar) by pulsed laser deposition (PLD) using a frequency doubled Nd:YAG laser (Quanta Ray GCR-5) with a wavelength of 532 nm and 10 Hz repetition rate. The films were deposited onto 10 x 10 mm and 22 x 22 mm glass slides (Agar Scientific borosilicate coverglasses), or 24 x 32 and 50 x 50 mm fused silica, which were baked out at 400 °C prior to the growth of the Fe₃O₄ layer at the same substrate temperature. The samples were then left to cool in vacuum until they reached room temperature, at which point the Pt layer was deposited. The Fe₃O₄ and Pt layers were deposited from stoichiometric Fe₂O₃ (Pi-Kem purity 99.9%) and elemental Pt (Testbourne purity 99.99%) targets using ablation fluences of 1.9 ± 0.1 and 3.7 ± 0.2 J cm⁻² respectively. The target to substrate distance was 110 mm. The Pt layer thickness was kept constant at 5 ± 0.5 nm for all films, whilst the substrate and Fe₃O₄ thicknesses were varied.

Bulk YIG was prepared by the solid state method. Stoichiometric amounts of Y₂O₃ and Fe₂O₃ starting powders (Sigma Aldrich 99.999% and 99.995% trace metals basis, respectively) were ground and mixed together before calcining in air at 1050 °C for 24 hours. Approximately 0.5g of the calcined powder was then dry pressed into a 13 mm diameter, 1.8 ± 0.2 mm thick cylindrical pellet. The pellet was then sintered at 1400 °C for 12 hours, after which, it was checked by XRD prior to sputtering 5 nm of Pt onto the as prepared surface using a benchtop Quorum turbo-pumped sputter coater. Samples were cut to size thereafter, using an IsoMet low speed precision cutter.

2.2 Structural characterization

XRD was obtained using a Bruker D2 Phaser in the standard Bragg-Brentano geometry using Cu K_α radiation; a Ni filter was used to remove the Cu K_β line. The samples were rotated at a constant 15 rpm throughout the scan to increase the number of crystallites being sampled. XRR measurements were taken using a modified Siemens D5000 diffractometer comprising a graphite monochromator reflecting only Cu K_α into the detector. The incident beam was collimated with a 0.05 mm divergence slit, while the reflected beam was passed through a 0.2 mm anti-scatter slit followed by a 0.1 mm resolution slit. XRR data was fitted using the GenX software package [2].

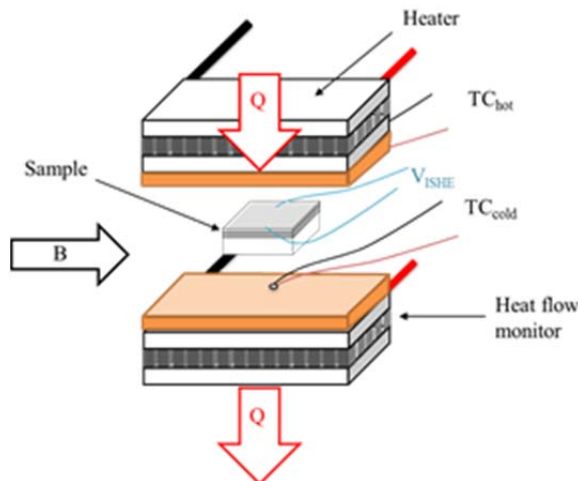


FIG. S1 Schematic of the spin Seebeck measurement system. Top and bottom Peltier cells act as heat source and heat flux monitor, respectively. Copper plates on the sample facing side of the Peltier cells provide high thermal conductivity at the interface, thus reducing lateral temperature gradients. GE varnish and mica are used to electrically isolate the copper surface from voltage contacts. Thermocouples monitor the temperature (with respect to the cold sink) at the top and bottom of the sample. Finally, the voltage, V_{ISHE} is monitored as Q and B are varied. Note that the thermal contact area, A_T , is defined as the area of sample connecting the top and bottom Peltier cells.

2.3 Magnetic and electric characterization

Magnetization as a function of applied magnetic field was measured using a Quantum Design Magnetic Properties Measurement System (SQUID). Several bilayer samples were characterized as a function of field at room temperature, whilst the Fe₃O₄ film (without Pt contact) was measured at 5 K, 100-130 K, and 295 K in order to observe the characteristic magnetic Verwey transition at 115 K.

Room temperature sheet resistance was obtained using the Van der Pauw method with a Keithley 6221/2182 nanovoltmeter and current source in conjunction with a Keithley 705 scanner.

2.4 Thermoelectric characterization

Spin Seebeck measurements were obtained from a set-up similar to that of Sola *et al.* [3], and outlined in Figure S1. There were 2 separate set-ups, optimized for 10x10 and 40x40 mm samples. The thin film was sandwiched between 2 Peltier cells, where the top Peltier cell (1) acted as a heat source, and the bottom Peltier cell (2) monitored the heat Q, through the sample. A copper sheet was affixed to the surface of the Peltier cells to promote uniform heat transfer.

Table S1 Summary of the thin film samples measured. The contact separation and corresponding thermal contact area, A_T , are also indicated. There were 2 distinct series of sample: (a) where the Fe₃O₄ and Pt thicknesses $t_{Fe_3O_4}$ and t_{Pt} were kept constant (at a nominal 80 nm:5 nm) and the substrate thickness $t_{substrate}$, was varied, and (b) where the Fe₃O₄ thickness was varied from 20 – 320 nm, whilst the Pt thickness was kept constant. Actual film thickness(es) were determined from fitting XRR data.

Sample	A_T (mm ²)	L_V (mm)	Substrate	$t_{substrate}$ (mm)	t_{Pt} (nm)	$t_{Fe_3O_4}$ (nm)
FP1	768	28.8	Glass	0.17	~4.8	80
FP3 (G6) (FP3 frag)	136.8 203	8.47 12.4	Glass	0.3	4.9	80
FP5 (G34)	484, 684, 880, 1530 214 270	19.3 19.3 7.62 19.44	Glass	0.5	5.5	80
FP6	772	28.56	Fused silica	0.67 0.67+0.67	4.8	80
FP9	983	36.66	Fused silica	0.9	5.4	80
F320P (G27)	66.6	6.58	Glass	0.3	4.4	320
F40P (G30)	100	6.26	Glass	0.3	5.2	40
F160P (G31)	100	5.5	Glass	0.3	4.5	160
F20P (G32)	100	7.25	Glass	0.3	5	20

Two type E thermocouples were mounted on the surface of these copper sheets such that they were in contact with the sample during the measurement. These thermocouples were connected in differential mode to monitor the temperature difference across the sample, ΔT .

The Peltier cells were calibrated by monitoring the Peltier voltage, V_p , generated as a current was passed through surface mount resistors fixed to the top side of the Peltier cell (where the sensitivity, S_p was found to be 0.067 - 0.12 V/W at 300K).

The heat flux, J_Q , is then determined by:

$$J_Q = V_p / (S_p A_T) \quad (S.1)$$

where A_T is the contact area between the top and bottom Peltier cells. This can be quickly related to the measured temperature difference ΔT , assuming that there are no major thermal losses or temperature drops at the sample:Peltier interface(s):

$$J_Q = k_{\text{eff}}\Delta T/L_z \quad (\text{S.2})$$

where k_{eff} is the effective thermal conductivity of the sample.

Given that this paper studies the impact of sample size (thus A_T is varied), it could be argued that for samples where A_T is less than the area of the top and bottom Peltier cells, there are significant thermal losses (radiation and convection). This is monitored by plotting the change in the measured J_Q as a function of ΔT , as was seen in Figure 1.

3 Results

3.1 Characterization of the Fe_3O_4 layer

Additional characterization data for the Fe_3O_4 thin films (deposited under identical conditions as the devices measured, but without the Pt top layer) is given in Fig. S2.

The Verwey transition is a characteristic feature of the Fe_3O_4 phase of iron oxide and manifests as a sharp increase in resistivity and hysteresis below the Verwey transition temperature (typically between 115 and 120 K)[1]. This feature is clearly seen in Fig. S2 (a), where magnetometry shows a sudden increase in hysteresis below 120 K.

In addition, XRD indicates a preference for $\langle 111 \rangle$ texture that is moderately sensitive to the direction of the plume during PLD (see repeated film depositions of Fig. S2 (c)). Due to the instability of the Fe_3O_4 phase, some Fe is also present. Finally, an example of the X-ray Reflectivity (XRR) fits used to obtain film thickness is given in Fig. S2 (d).

3.2 Characterization of the Fe_3O_4 :Pt bilayers

Additional characterization data for the Fe_3O_4 :Pt bilayers is given in Fig. S3. Previous work showed that for $t_{\text{Pt}} > 2$ nm a thin continuous paramagnetic Pt layer deposited on top of the Fe_3O_4 layer follows the wavy surface of the Fe_3O_4 layer. The Pt stacks on top of the Fe_3O_4 (111) planes and the two grains have an orientation relationship of $[011]_{\text{Pt}}/[011]_{\text{Fe}_3\text{O}_4}$, $(111)_{\text{Pt}}/(111)_{\text{Fe}_3\text{O}_4}$, which minimizes the interface energy due to minimal lattice mismatch of $d(111)_{\text{Pt}}$ (0.226 nm; JCPDS card 4-802) and $d(222)_{\text{Fe}_3\text{O}_4}$ (0.242 nm; JCPDS card 19-629).

XRD data for the sample series where the Fe_3O_4 and substrate thickness was varied is given in Fig. S3. For the substrate study, XRR indicated similar Pt thickness (low frequency ‘bumps’ in the data) as well as some variation in the interface quality (whether high frequency fringes can be observed indicates the relative roughness of the substrate, Fe_3O_4 and Pt layers). Fig. S3 also shows the XRD and magnetization measurements of the sample series where the Fe_3O_4 thickness was varied. Of particular note is the saturation of the magnetic moment of Fe_3O_4 measured at 1 T for thicknesses > 80 nm.

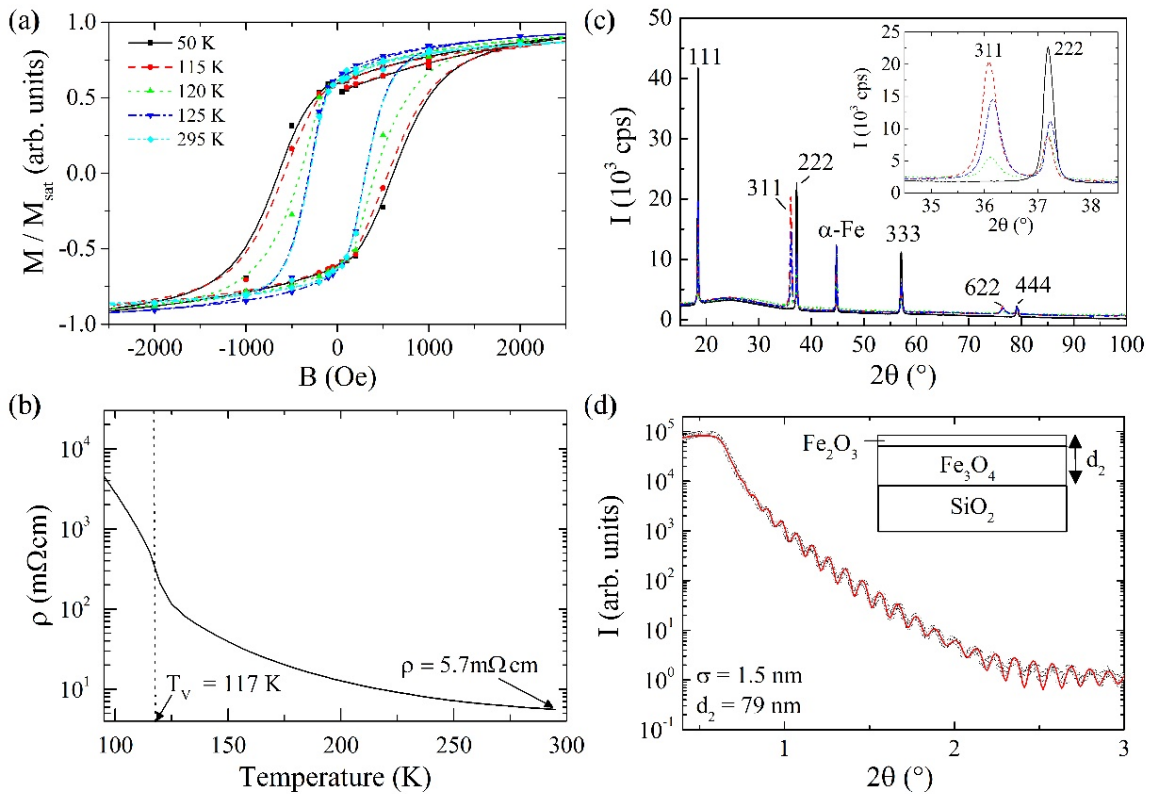


FIG. S2 Characterization of the Fe_3O_4 film. a) SQUID magnetometry above and below the Verwey transition, T_V . b) Resistivity as a function of temperature. c) XRD of a set of 4 separately prepared Fe_3O_4 films. The inset shows a close-up of the (311), (222) peaks. d) Example XRR data (symbols) and fit (solid line), indicating thickness = 79 nm, roughness = 1.5 nm.

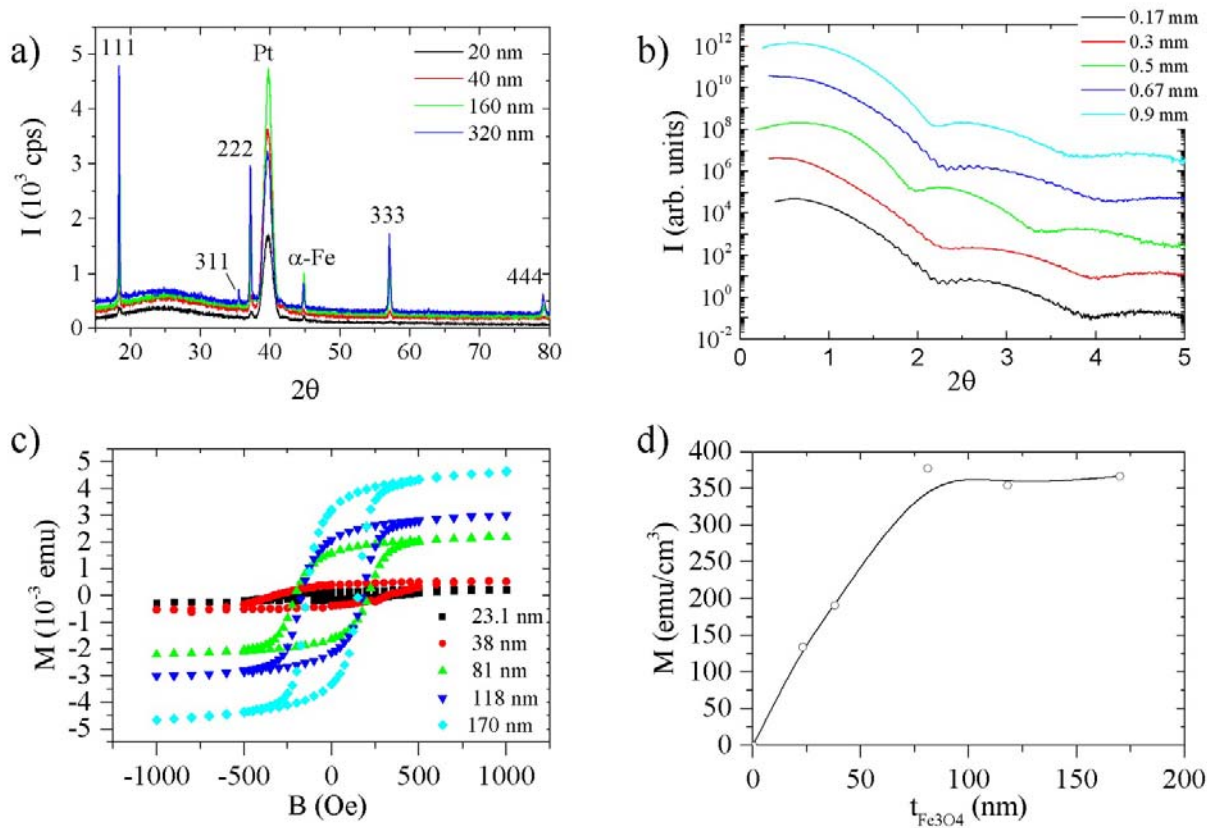


FIG. S3 Characterization of the Fe_3O_4 :Pt films, where Fe_3O_4 and substrate thickness was varied. a) XRD for Fe_3O_4 thickness study, b) XRR for substrate study, and c) SQUID magnetometry as a function of Fe_3O_4 thickness. d) Saturation magnetisation, M , as a function of Fe_3O_4 thickness.

3.3 Characterization of YIG

XRD of the YIG pellet presented here is given in Figure S4. No evidence of unreacted starter powders (Fe_2O_3 , Y_2O_3) or potential secondary phase YIP (YFeO_3) was seen, as highlighted in Figure S4(b). Scanning electron microscopy images show grain structure with a porosity expected from 30% estimated open porosity as measured by the Archimedes method.

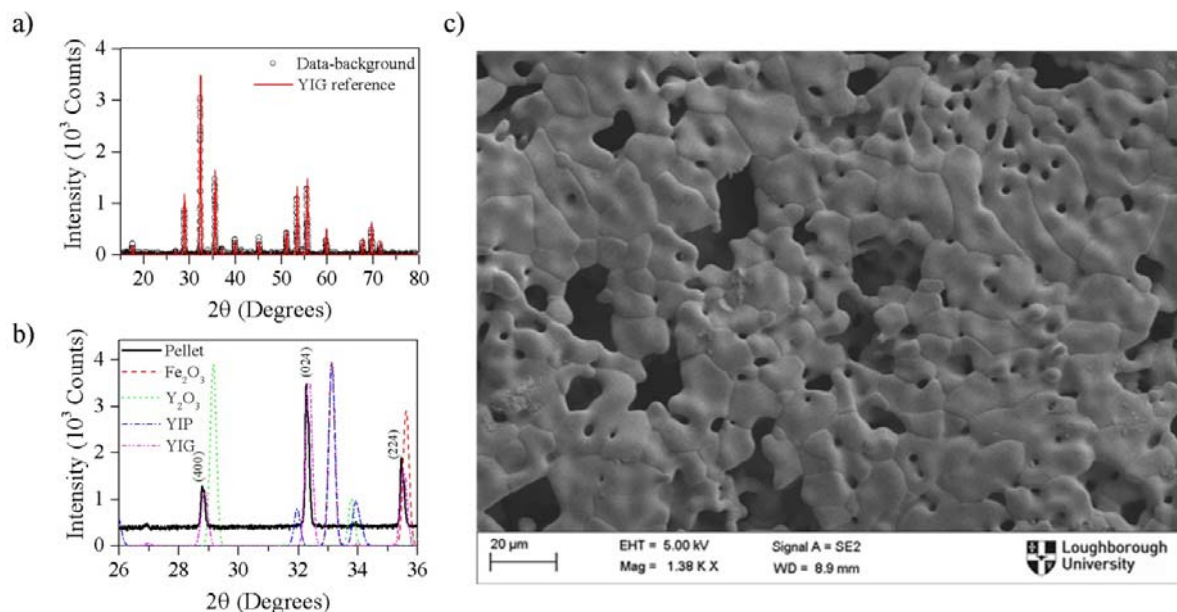


FIG. S4 (a)&(b) X-ray diffraction data for the YIG pellet. (a) Normalized data alongside reference for $\text{Y}_3\text{Fe}_5\text{O}_{12}$ (YIG). (b) Zoomed in data selection plotted alongside possible impurity phases Fe_2O_3 and Y_2O_3 (starting powders) and YFeO_3 (YIP). (c) Scanning Electron Microscope image of the pellet, where grain size was found to be an average of $14.5 \mu\text{m}$, with open porosity of 30%.

3.4 Additional spin Seebeck data

Fig. S5 shows the results of the scribing study, where A_T was fixed, but L_x , L_y (not L_x^T , L_y^T) were varied by scribing away sections of the thin film, as illustrated in Fig. S5(a). In this case, the voltage always scaled with the contact separation, L_y , indicating that the behavior we see is not due to a change in the film properties (such as resistance), but scaling of the heat flux.

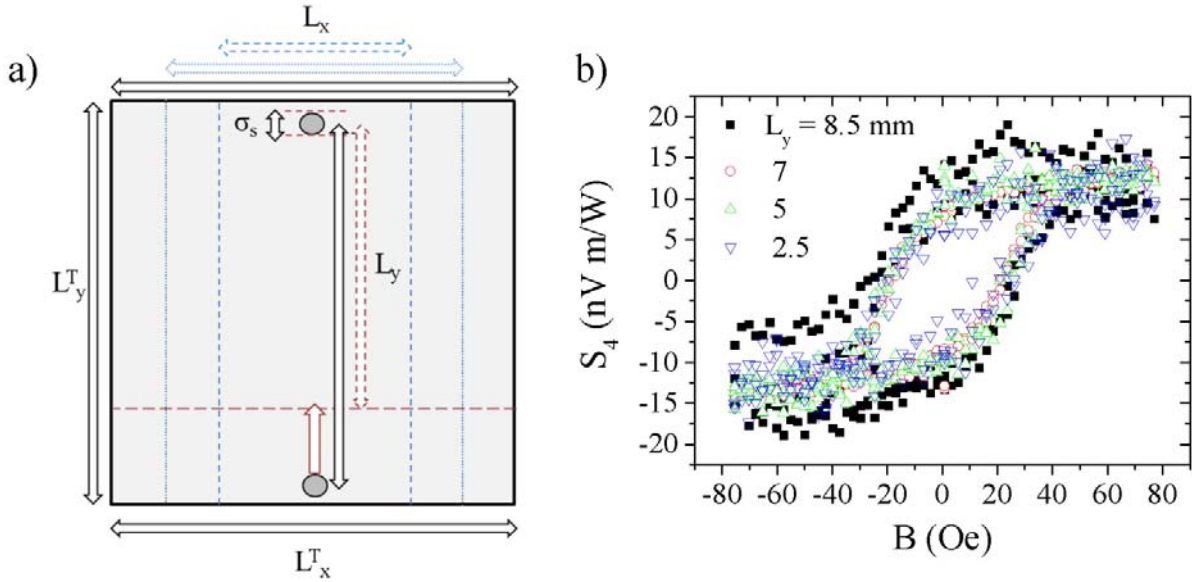


FIG. S5 Results of the scribing study. As long as A_T was unchanged, as L_x and L_y were varied (by scribing away the sample such that it is still thermally connected, but electrically isolated), the voltage always scaled the same. Large noise is due to reducing contact separation and additional electrical noise during some of the measurements (due to a loose wire).

References

- [1] F. Walz, *J. Phys. Condens. Mat.* **14**, R285-R340 (2002).
- [2] M. Björck, and G. Andersson, *J. Appl. Cryst.* **40**, 1174-1178 (2007).
- [3] A. Sola, M. Kuepferling, V. Basso, M. Pasquale, T. Kikkawa, K. Uchida, and E. Saitoh, *J. Appl. Phys.* **117**, 17C510 (2015)